JACS
JOURNAL OF THE AMERICAN CHEMICAL SOCIETY
Article
pubs.acs.org/JACS

Transient B_{12}-Dependent Methyltransferase Complexes Revealed by Small-Angle X-ray Scattering

Nozomi Ando,[†,‡] Yan Kung,[‡] Mehmet Can,[∥] Güneş Bender,[∥] Stephen W. Ragsdale,[∥] and Catherine L. Drennan*[,†,‡,§]

[†]Howard Hughes Medical Institute, [‡]Department of Chemistry, and [§]Department of Biology, Massachusetts Institute of Technology, Cambridge, Massachusetts 02139, United States

[∥]Department of Biological Chemistry, University of Michigan, Ann Arbor, Michigan 48109, United States

Supporting Information

ABSTRACT: In the Wood–Ljungdahl carbon fixation pathway, protein–protein interactions between methyltransferase (MeTr) and corrinoid iron–sulfur protein (CFeSP) are required for the transfer of a methyl group. While crystal structures have been determined for MeTr and CFeSP both free and in complex, solution structures have not been established. Here, we examine the transient interactions between MeTr and CFeSP in solution using anaerobic small-angle X-ray scattering (SAXS) and present a global analysis approach for the deconvolution of heterogeneous mixtures formed by weakly interacting proteins. We further support this SAXS analysis with complementary results obtained by anaerobic isothermal titration calorimetry. Our results indicate that solution conditions affect the cooperativity with which CFeSP binds to MeTr, resulting in two distinct CFeSP/MeTr complexes with differing oligomeric compositions, both of which are active. One assembly resembles the CFeSP/MeTr complex observed crystallographically with 2:1 protein stoichiometry, while the other best fits a 1:1 CFeSP/MeTr arrangement. These results demonstrate the value of SAXS in uncovering the rich solution behavior of transient protein interactions visualized by crystallography.

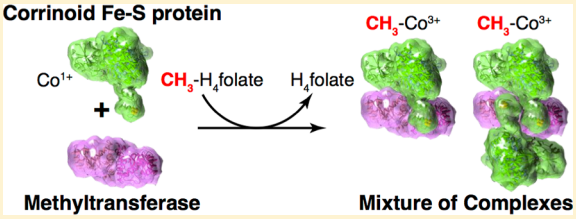

INTRODUCTION

The Wood–Ljungdahl pathway in acetogenic bacteria is estimated to produce 10^{12} kg of acetate annually from environmental CO_2 and other carbon sources.[1,2] As shown in Figure 1A, this pathway involves nine enzymes working together to convert two molecules of CO_2 and coenzyme A (CoA) into acetyl-CoA,[2] which can subsequently be assimilated as cell carbon or converted to acetate and other products, such as ethanol or butanol, depending on the acetogenic strain.[3] Harnessing the ability of acetogens to produce commercially useful multicarbon compounds from CO_2 has long been of interest to the biotechnology community.[3−6] In this study, we investigate protein–protein interactions that are responsible for the hand-off of one-carbon units from one enzyme to the next in the Wood–Ljungdahl pathway of the model acetogen *Moorella thermoacetica*. We focus on two of the key enzymes in this pathway: the methyltransferase (MeTr) and the corrinoid iron–sulfur protein (CFeSP), which must interact to catalyze the transfer of a one-carbon methyl unit. This interaction is known to be weak, with values of 12–60 μM reported for the Michaelis constant, K_M.[7,8] With recent X-ray structures providing static snapshots of the interactions between these two proteins,[9] we can now probe their solution structures and investigate their transient interaction in different chemical environments using small-angle X-ray scattering (SAXS).

The interaction between MeTr and CFeSP lies at a crucial junction in the Wood–Ljungdahl pathway. In the so-called Eastern branch of the pathway, a series of folate-dependent enzymes catalyzes the reduction of one CO_2 to the methyl group of methyltetrahydrofolate (CH_3-H_4folate). The Western branch of the pathway begins with MeTr, which binds CH_3-H_4folate and transfers the methyl group to the cobalt center of a vitamin B_{12} derivative (5′-methoxybenzimidazolyl cobamide) harbored by CFeSP. To enable this first B_{12}-dependent methyl transfer step, the direct interaction between CFeSP and MeTr is required to position the cobalt center of the B_{12} cofactor within bonding distance of the methyl group from CH_3-H_4folate. Crystallographic analysis has revealed that MeTr from *M. thermoacetica* is a 57 kDa homodimer of $(\beta/\alpha)_8$ triosephosphate isomerase (TIM) barrels, each of which may bind one molecule of CH_3-H_4folate,[10,11] while CFeSP is an 83 kDa heterodimer consisting of a small subunit with a TIM barrel fold and a large subunit with three domains connected by linkers: an N-terminal domain that harbors an Fe_4S_4 cluster, a central TIM barrel domain, and a C-terminal B_{12}-binding domain (Figure 1B).[9] Crystal structures of CFeSP/MeTr complexes show that two CFeSPs are bound to a central MeTr homodimer (Figure 1C). Together, these interactions lead to a catalytically competent domain arrangement, in which the B_{12} domain is able to swing freely from a resting state, where reactive B_{12} species (Co(I) and CH_3-Co(III)) are protected by the CFeSP small subunit, to a catalytic state, where B_{12} is positioned above the MeTr active site for methyl transfer.[9,12,13]

Received: June 14, 2012
Published: October 9, 2012

dx.doi.org/10.1021/ja3055782 | J. Am. Chem. Soc. 2012, 134, 17945−17954

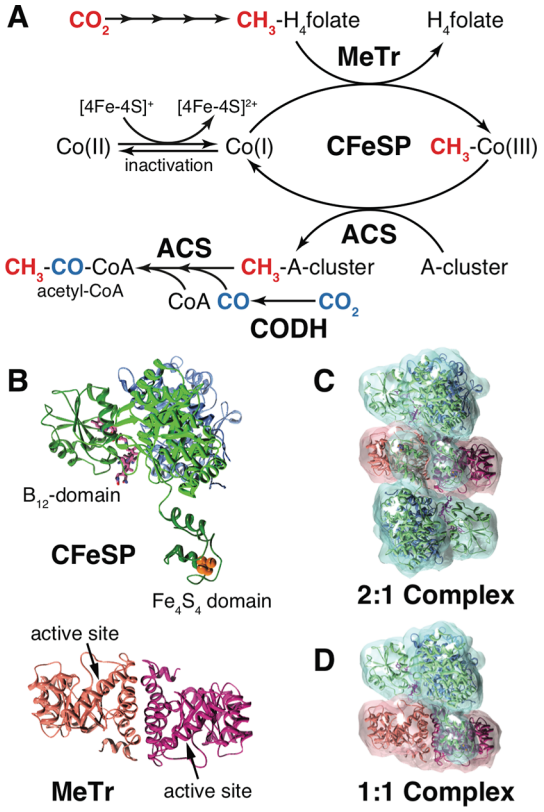

Figure 1. CFeSP and MeTr in the Wood–Ljungdahl carbon fixation pathway. (A) One molecule of CO_2 (red) is reduced to a methyl group in a series of folate-dependent reactions, catalyzed by five enzymes, to produce CH_3-H_4folate, the substrate of MeTr. MeTr and B_{12}-containing CFeSP form a complex to transfer the methyl group to the Co(I) center of the B_{12} cofactor, forming a CH_3–Co(III) intermediate. CFeSP then delivers the methyl group to the Ni–Fe–S A-cluster of ACS, reducing the B_{12} cobalt back to the Co(I) state. ACS subsequently catalyzes formation of acetyl-CoA by combining the methyl group with CoA and CO, itself derived from a second molecule of CO_2 (blue) by the action of carbon monoxide dehydrogenase (CODH). Intermittent oxidation of the reactive Co(I) state of B_{12} causes inactivation to the Co(II) state. CFeSP can be reactivated by an electron that is transferred from the CFeSP Fe_4S_4 cluster to the B_{12} cobalt. (B) CFeSP is a heterodimer of a small (light blue) and a large (green) subunit consisting of a B_{12}, central, and Fe_4S_4 domain.[9] MeTr is a homodimer (pink/magenta), with each monomer containing a CH_3-H_4folate binding site.[10,11] (C) Crystal structures of CFeSP/MeTr in complex exhibit 2:1 stoichiometry, with CFeSP (cyan) making equivalent interactions on either side of MeTr (pink).[9] (D) A model for a CFeSP/MeTr complex with 1:1 stoichiometry can be generated by removing one CFeSP from the structure shown in (C).

To complement these crystallographic data and explore the interactions of *M. thermoacetica* CFeSP/MeTr components under different solution conditions, we employed anaerobic SAXS. SAXS is a solution-based structural technique that can provide both stoichiometric and structural information in the analysis of multispecies systems.[14−16] Deconvolution of multispecies SAXS data, however, is complicated by the challenges of obtaining high-quality data while avoiding overinterpretation.[17] Here, we present a global analysis approach for the deconvolution of mixtures formed by weakly interacting proteins of known structure and further support this analysis with isothermal titration calorimetry (ITC). Our results show that under all protein concentrations tested, MeTr maintains homodimeric association, while CFeSP remains a heterodimer of large and small subunits. Unexpectedly, however, when CFeSP and MeTr are mixed, two distinct CFeSP/MeTr complexes are observed with different subunit compositions, whose distributions are dependent upon the solution conditions. These results highlight the utility of SAXS in gaining unique insight into the solution behavior of transient protein–protein interactions observed by crystallography.

RESULTS

Solution Conformations of Free MeTr and CFeSP. Prior to the characterizations of MeTr and CFeSP in complex, SAXS measurements were made of free MeTr and CFeSP under previously established *in vitro* assay conditions (50 mM Tris-HCl pH 7.6, 100 mM NaCl, 2 mM dithiothreitol)[18] at protein concentrations near the physiological value[7] of ∼50 μM (corresponding to mass per volume concentrations of 2.9 and 4.2 mg/mL for MeTr and CFeSP, respectively). To assess data quality and determine the overall radius of gyration, R_g, which is a function of spatial size, the obtained data were plotted as Guinier curves, $\ln(I)$ versus q^2, where I is the scattering intensity and q is a function of scattering angle.[19] The resultant Guinier curves display linearity at low q (Figure 2A,B), indicating that for both proteins R_g (determined from the slope) is well-defined at all concentrations and that interparticle effects, including those associated with radiation damage, are negligible. Molecular weight determination from these data by a Porod invariant method[20] gave 53 and 83 kDa for MeTr and CFeSP, respectively, in excellent agreement with the actual values of 57 kDa for MeTr homodimer and 83 kDa for CFeSP heterodimer determined from their protein sequences and metal compositions.[21,22]

For both proteins, minimal concentration dependence was observed in R_g, indicating that their respective oligomerization states do not change over the investigated ranges (Figure 2C,D). Linear extrapolation to infinite dilution[19] yields an R_g value of 27.6 ± 0.4 Å for MeTr, in good agreement with the theoretical value of 26.9 Å calculated from the previously reported crystal structure of the MeTr homodimer.[11] Furthermore, the theoretical scattering profile calculated from the crystal structure generates an excellent fit to the experimental scattering data (Figure 3A, black solid curve). Likewise, the extrapolated R_g value of 31.1 ± 0.7 Å for CFeSP is consistent with the theoretical value calculated from the previously reported structure of a homologous CFeSP from *Carboxydothermus hydrogenoformans*[12] (30.2 Å) as well as those calculated from individual CFeSPs extracted from structures of the *M. thermoacetica* CFeSP/MeTr complex (30.1–30.4 Å).[9] While these CFeSP structures depict the B_{12} and Fe_4S_4 domains in different positions (Figure 3C), consistent with the mechanistic proposals that require domain movements for catalysis,[9,12,13] all structural models generate excellent fits to the experimental scattering up to a maximum q of 0.25 Å^{-1}, suggesting that they are nearly indistinguishable at this resolution (25 Å) (Figure 3B). Ensemble fitting was not attempted in order to avoid overinterpretation of the data. Instead, a CFeSP model extracted from the crystal structure of the folate-free CFeSP/MeTr complex[9] which provided a slightly better fit over the others was used in the following analyses (Figure 3B).

Three-dimensional *ab initio* molecular envelopes for both MeTr and CFeSP were reconstructed from SAXS data collected at 100 μM protein concentration (Table 1). The crystal structure of homodimeric MeTr[11] fits well into the elongated

dx.doi.org/10.1021/ja3055782 | J. Am. Chem. Soc. 2012, 134, 17945−17954

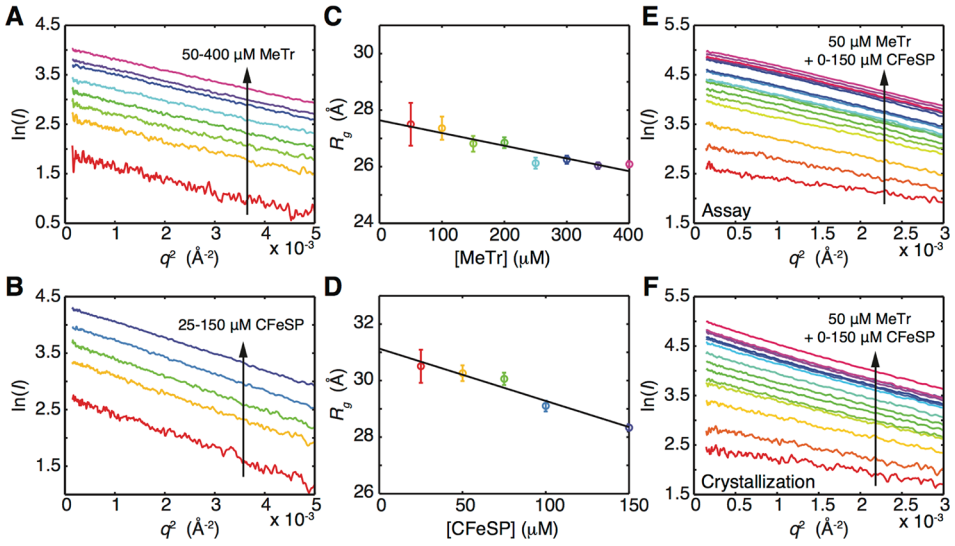

Figure 2. Guinier analysis of MeTr and CFeSP on their own and mixed. (A) Guinier plot of 50−400 μM MeTr under assay conditions. (B) Guinier plot of 25−150 μM CFeSP under assay conditions. (C,D) The corresponding radii of gyration (R_g) determined from the slopes of the Guinier plots are linear with respect to protein concentration. Linear extrapolation to infinite dilution gives R_g values of 27.6 ± 0.4 and 31.1 ± 0.7 Å for MeTr and CFeSP, respectively, in good agreement with theoretical values determined from crystal structures.[9,11] (E) Guinier plot for the CFeSP titration (0−150 μM) into MeTr homodimer (fixed at 50 μM) under assay conditions. (F) Guinier plot for same titration as in (E) but under crystallization conditions. All Guinier plots show linearity in this low q range.

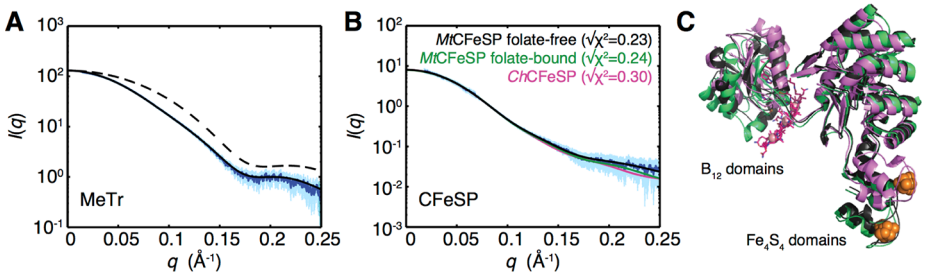

Figure 3. Model fitting to the scattering of free MeTr and CFeSP under assay conditions. (A) The theoretical profile (black solid) of the homodimeric *M. thermoacetica* MeTr crystal structure[11] fits well to experimental data obtained from 470 μM MeTr (dark blue with error bars shown in cyan), while that of just one MeTr monomer (black dashed) gives a poor fit. (B) Theoretical profiles of the three CFeSP models (shown in C, with same coloring) are nearly superimposable with each other at 25 Å resolution (i.e., q < 0.25 Å^{-1}). *Mt*CFeSP from the folate-free structure[9] provides the best fit (lowest $\sqrt{\chi^2}$) to the experimental curve (dark blue with error bars shown in cyan) obtained by merging low q data from 19 μM CFeSP, which exhibited minimal interparticle effects, and high q data from 230 μM CFeSP. (C) Crystal structures depict CFeSP in three different conformational states: *M. thermoacetica* CFeSP (*Mt*CFeSP) extracted from structures of CFeSP/MeTr in the folate-free (black ribbons) and folate-bound (green ribbons) states[9] and a structure of a homologous CFeSP from *Carboxydothermus hydrogenoformans* (*Ch*CFeSP) (pink).[12] When aligned by the small subunit (light blue in Figure 1B but not shown here for clarity), these structures differ most in the positions of the mobile B_{12} (magenta sticks) and Fe_4S_4 (orange spheres) domains due to their inherent mobility.

molecular envelope for this protein (Figure 4A). The reconstructed envelope of CFeSP features three lobes, which align well with the core domains of CFeSP, composed of the small and large subunit TIM barrels and the B_{12} domain (Figure 4B). Unsurprisingly, the mobile Fe_4S_4 domain, which has only been visualized crystallographically with stabilizing intermolecular contacts,[9,12,13] was not visible in this averaged model obtained by SAXS. While small disordered features are observed in the individual shape reconstructions that could represent the Fe_4S_4 domain in multiple conformations (Figure S1), the loss of these features with averaging is consistent with the absence of a localized position for this domain.

Relative Molar Concentrations of Subunits. For the accurate stoichiometry determination of CFeSP and MeTr in complex, the relative molar concentrations of the individual subunits must be well-defined. The molar ratio of the protein stock solutions was therefore determined spectroscopically by the Rose−Bengal method[23] and confirmed with the zero-angle scattering intensity, $I(0)$, determined by SAXS. When the oligomerization state is known, $I(0)$ is approximately proportional to the molar protein concentration, c, and the molecular weight squared, MW^2.[24] $I(0)$ was determined from linear fits to Guinier curves for each protein at three different protein concentrations under assay conditions. For both proteins, $I(0)$/MW^2 values derived from SAXS show a linear relationship with c, determined spectroscopically (Figure 5), confirming that their respective oligomerization states do not change with protein concentration. Furthermore, the plots for MeTr and CFeSP share the same slope, indicating that the molar ratio of the two proteins is consistent between the spectroscopic assay and SAXS.

Complex Formation under Assay Conditions. To characterize complex formation by SAXS, simply mixing the components at the expected stoichiometries is insufficient for a

dx.doi.org/10.1021/ja3055782 | J. Am. Chem. Soc. 2012, 134, 17945−17954

Table 1. Shape Reconstruction Statistics[a]

	MeTr	CFeSP	1:1 complex
figure	4A	4B	4C
protein concentration (μM)	100	100	150
q range (Å^{-1})	0.015−0.229	0.022−0.221	0.031−0.238
real space range (Å)	0−88	0−90	0−100
GNOM total estimate	0.633	0.669	0.742
shape reconstruction	dammif 1.1.1	dammif 1.1.1	dammif 1.1.0
symmetry	$P2$	$P1$	$P1$
$\sqrt{(\chi^2)}$	2.188−2.197	2.145−2.146	1.185−1.186
no. of models averaged/total	20/20	19/20	10/10
Damaver NSD (var.)	0.992 (0.269)	0.669 (0.043)	0.811 (0.048)

[a]All measurements were under assay conditions (50 mM Tris-HCl pH 7.6, 100 mM NaCl, 2 mM dithiothreitol). Experimental scattering profiles were converted into inputs for shape reconstructions in GNOM with reasonable total estimate scores.[28]

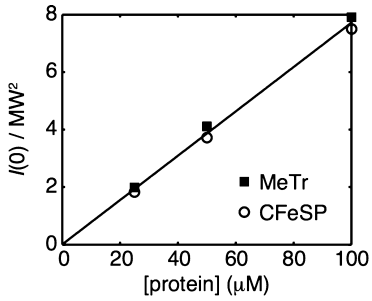

Figure 5. Correlation of relative MeTr and CFeSP concentrations obtained by SAXS with those obtained spectroscopically. The molecular-weight-normalized forward scattering intensities from SAXS, $I(0)/MW$,[2] linearly correlate with the spectroscopically determined molar concentration, c, indicating that oligomerization states do not change with increasing protein concentrations. Points for MeTr and CFeSP are nearly colinear, indicating that their SAXS-derived and spectroscopically determined relative concentrations are in agreement.

number of reasons. As protein associations are concentration dependent, single measurements may not capture a homogeneous solution of fully associated complexes, and the polydispersity of a solution cannot be easily determined from single scattering profiles. Furthermore, complexes may adopt unanticipated subunit stoichiometries in solution. Finally, there is a danger of overfitting multicomponent data.

Therefore, to investigate the complex formation of CFeSP and MeTr, we generated a series of scattering curves collected over a subunit titration experiment and implemented a global analysis approach to identify the minimum set of species represented by the data. CFeSP was titrated into 50 μM MeTr under assay conditions such that the molar ratio of the two proteins spanned a wide range. Reasonable linearity was observed in the resultant Guinier curves (Figure 2E), indicating that the solutions can be considered dilute and absent of radiation damage and, hence, that the scattering profiles can be approximated as linear combinations of the scattering contributions of individual species.

In our global analysis, an ensemble of possible species is first generated based on experimentally known structures. Theoretical scattering curves of these species are calculated from atomic coordinates in CRYSOL,[25] and all possible linear combinations are fit to the titration data in OLIGOMER.[26] The significant species present in the data are identified by determining the minimum subensemble that satisfies three criteria. First, the goodness-of-fit parameter, χ^2, must be both globally minimized (i.e., across the entire titration) as well as be meaningfully reduced relative to other subensembles. Since increasing the number of species in a fit often leads to a better fit, the latter condition prevents overfitting. Second, the residuals from the fits must be flattened across the entire data set (i.e., show no significant dependence on q or the molar ratio of the subunits). Finally, the resultant volume fractions of each species from the fits must show physically reasonable dependence on the molar ratios of the subunits. Because fitting sums of scattering form

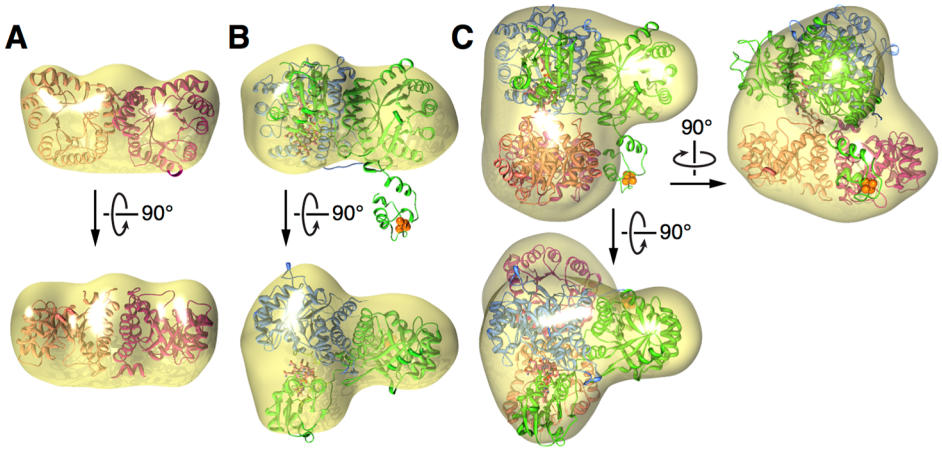

Figure 4. SAXS-derived *ab initio* shape reconstructions depicting solution conformations of MeTr and CFeSP, free and in complex under assay conditions. (A) The molecular envelope reconstructed from 100 μM MeTr aligns well with the crystal structure of the homodimer,[11] shown as pink and orange ribbons. (B) Likewise, the molecular envelope of 100 μM CFeSP aligns well with a CFeSP structure extracted from a crystal structure of the CFeSP/MeTr complex,[9] shown as blue and green ribbons for the small and large subunits, respectively. The Fe_4S_4 cluster is shown as orange spheres and B_{12} in magenta sticks. (C) The molecular envelope reconstructed from a 150 μM equimolar solution of the CFeSP heterodimer, and the MeTr homodimer aligns well with the core domains of the 1:1 complex (ribbons, same coloring as in (A,B)). Shape reconstructions statistics are provided in Table 1.

dx.doi.org/10.1021/ja3055782 | J. Am. Chem. Soc. 2012, 134, 17945−17954

factors to experimental data does not take into account subtle interparticle interactions, we emphasize that the volume fractions are apparent and should not be taken as precise quantities. In particular, errors arise due to interparticle excluded volume effects, which lead to apparent decreases in R_g that are manifested as an underestimation in the volume fraction of large species and an overestimation in the fraction of small species. In our global analysis approach, overinterpretation of the data is thus avoided by considering trends in apparent volume fractions rather than the individual values for any single scattering curve.

For fitting the titration data, an ensemble of four possible species was considered, including the three crystallographically observed species: a "2:1 complex" as depicted in the CFeSP/MeTr crystal structures,[9] where two CFeSP heterodimers are bound to one central MeTr homodimer (Figure 1C), and the uncomplexed proteins, which, as described above, are represented well by a MeTr crystal structure[11] and a CFeSP model extracted from a CFeSP/MeTr crystal structure,[9] respectively (Figures 3 and 4A,B). Because the CFeSP/MeTr crystal structures show that each CFeSP binds to analogous sites on either side of the MeTr homodimer, a "1:1 complex" in which only a single CFeSP is bound to the MeTr homodimer was also included in the ensemble (Figure 1D).

Different linear combinations of the four species were fit to the titration data over the q range 0.018−0.160 Å^{-1}, and the $\sqrt{\chi^2}$ values reported by OLIGOMER[26] are shown in Figure 6. As expected, linear combinations of the uncomplexed proteins alone generate poor fits to the data (Figure 6A, black circles).

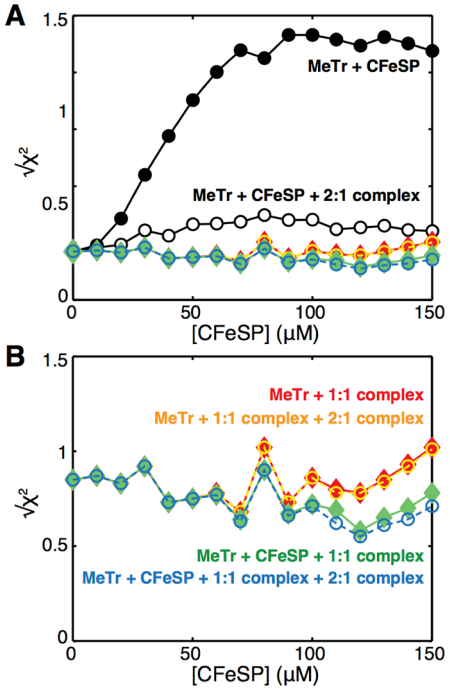

Figure 6. Global χ^2 minimization of multispecies fitting to scattering data obtained in the titration of CFeSP (0−150 μM) into MeTr homodimer (fixed at 50 μM) under assay conditions. (A) Fits shown include: free MeTr + free CFeSP (black circles), free MeTr + free CFeSP + 2:1 complex (white circles), free MeTr + 1:1 complex (red diamonds), free MeTr + 1:1 complex + 2:1 complex (orange circles), free MeTr + free CFeSP + 1:1 complex (green diamonds), and free MeTr + free CFeSP + 1:1 complex + 2:1 complex (blue circles). (B) Close up of colored curves in (A).

While fitting the 2:1 complex with the uncomplexed proteins reduces the $\sqrt{\chi^2}$ values (Figure 6A, white circles), the residuals display significant q dependence (Figure S2, top). Significant $\sqrt{\chi^2}$ reduction is observed when the 1:1 complex is included in the linear combinations (colored curves in Figure 6A and close up in 6B), particularly at high [CFeSP], suggesting that complex formation cannot be adequately described without this species. Here, a three-species fit consisting of the uncomplexed proteins and the 1:1 complex leads to both low $\sqrt{\chi^2}$ values (Figure 6B, green diamonds) and low residuals (Figure S2, middle), while the addition of the 2:1 complex to this combination leads to only negligible changes in the goodness of fit (Figure 6B, blue circles and Figure S2, bottom). By comparison, omitting free CFeSP from these linear combinations has a greater effect with respect to $\sqrt{\chi^2}$ values (Figure 6B, red diamonds and orange circles) than omitting the 2:1 complex. Together, these results suggest that only three significant species are present under these conditions: free MeTr, free CFeSP, and the 1:1 complex. The assignment of three significant species under assay conditions is further supported by singular value decomposition (SVD) analysis, a model-independent matrix factorization method[14,24] (Figure S3A).

Linear combinations of free MeTr, free CFeSP, and the 1:1 complex generate excellent fits to the scattering profiles (Figure 7A), and the corresponding apparent volume fractions display physically reasonable trends over the course of the titration (Figure 7C). As CFeSP is added, free MeTr is consumed to form the 1:1 complex. The 1:1 complex is maximally formed at equimolar concentrations of CFeSP and MeTr homodimer (Figure 7C, dotted line), consistent with the equimolar subunit stoichiometry. Likewise, the volume fractions of the uncomplexed proteins intersect near the equimolar point. These physically reasonable trends are obtained by fitting just three species, consistent with the SVD and $\sqrt{\chi^2}$ analysis described above. When a fourth species, the 2:1 complex, is included in the fitting, the resultant volume fractions for this species are negligible, as expected (Figure S4B). Thus, instead of forming a 2:1 complex to any appreciable extent, a buildup of unbound CFeSP is observed in the presence of excess CFeSP (Figure 7C and S4B). Importantly, physically reasonable trends are lost when incorrect combinations of species are fit. For example, a three-species fit with the 2:1 complex and the uncomplexed proteins results in a physically impossible trend with maximum free CFeSP at low CFeSP concentrations (Figure S4A).

To deconvolute interparticle effects from the SAXS data, equimolar mixtures of CFeSP heterodimer and MeTr homodimer were diluted from 150 to 25 μM under assay conditions. A slight and linear increase in R_g is observed with dilution, consistent with the release of interparticle excluded volume effects (Figure 8, red). Linear extrapolation to infinite dilution yields an R_g of 35.5 ± 0.5 Å, which is in excellent agreement with the theoretical value of 34.5 Å for the 1:1 complex, while much smaller than the theoretical R_g for the 2:1 complex of 43.5 Å. Likewise, a molecular envelope reconstructed from data collected at 150 μM agrees well with the model of the 1:1 complex (Figure 4C). Only the B_{12} and Fe_4S_4 domains protrude slightly from the reconstruction density, again consistent with the CFeSP/MeTr crystal structures, where these domains are mobile, exhibiting higher crystallographic *B*-factors and weaker electron density.[9] These results suggest that under assay conditions, the 1:1 complex is largely associated at the examined protein concentrations. By

dx.doi.org/10.1021/ja3055782 | J. Am. Chem. Soc. 2012, 134, 17945−17954

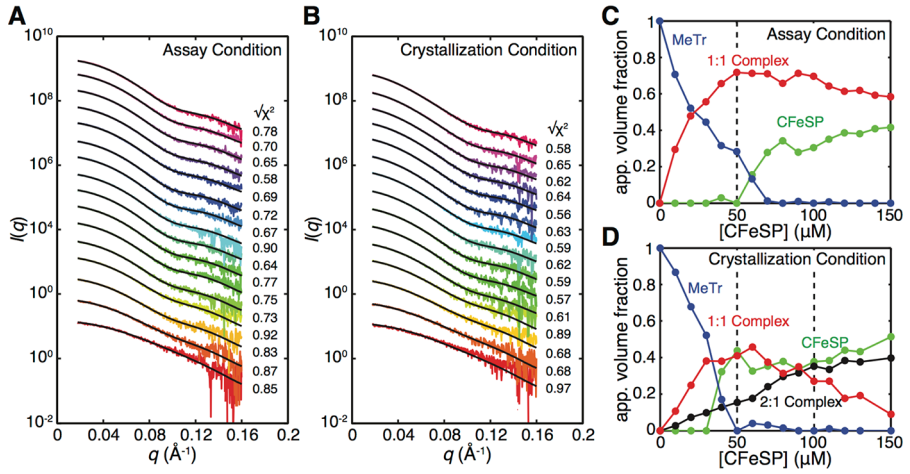

Figure 7. Determination of subunit stoichiometry in the complex formation of MeTr and CFeSP. (A) Scattering profiles for the titration of 0−150 μM CFeSP into MeTr homodimer (50 μM) under assay conditions. Profile colors range from red to violet (bottom to top) and indicate increasing CFeSP concentrations. Linear combinations of free MeTr, free CFeSP, and the 1:1 complex fitted to the data (shown in black) and corresponding $\sqrt{\chi^2}$ values were obtained with the program OLIGOMER.[26] (B) Scattering profiles for the titration described in (A) but under crystallization conditions fitted with linear combinations of free MeTr, free CFeSP, the 1:1 complex, and the 2:1 complex (black). (C) Plot of deconvolution results for CFeSP titration performed under assay conditions. Blue circles represent free MeTr homodimer, green circles represent free CFeSP heterodimer, and red circles represent the 1:1 complex (Figure 1D). Dashed vertical lines are visual guides for 50 and 100 μM CFeSP concentrations. (D) Plot of deconvolution results for CFeSP titration under crystallization conditions, with symbols and lines as described in (C). Black circles represent the 2:1 complex. The volume fractions are apparent values (see text).

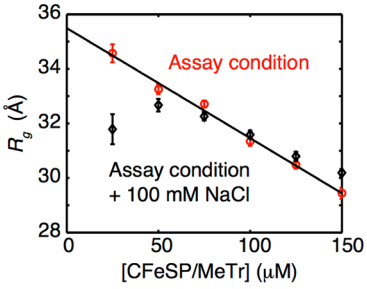

Figure 8. R_g concentration dependence in presence of 25−150 μM equimolar mixtures of the CFeSP heterodimer with the MeTr homodimer. Under assay conditions (red circles), the R_g values show a slight linear decrease with increasing concentration, indicating that neither dissociation nor higher order oligomerization occurs over this concentration range. Linear extrapolation to zero concentration to eliminate volume exclusion effects gives R_g of 35.5 ± 0.5 Å, which agrees well with the theoretical value of 34.5 Å for the 1:1 complex (Figure 1D). Increasing the ionic strength to a total NaCl concentration of 200 mM (black diamonds) leads to partial dissociation below protein concentrations of 50 μM. Above 50 μM, the R_g values follow the same trend as that seen under assay conditions, suggesting that the 1:1 CFeSP/MeTr complex is favored even at increased ionic strength.

comparison, when the NaCl concentration is increased by an additional 100 mM (to a final concentration of 200 mM), R_g decreases nonlinearly at protein concentrations below 50 μM, indicative of subunit dissociation (Figure 8, black). The sensitivity to ionic strength also suggests the presence of a salt bridge contributing to the stability of the 1:1 complex.

Thermodynamics of Negative Cooperativity under Assay Conditions. Surprisingly, the preference for the formation of the 1:1 complex over the 2:1 complex observed under assay conditions implies that the binding of CFeSP to one of two equivalent sites on the MeTr homodimer disfavors binding of the second CFeSP. To test for the presence of negative cooperativity, anaerobic ITC was performed under assay conditions, and data from multiple subunit titration experiments were globally fit with the program Sedphat.[27] When binding of two CFeSPs to MeTr is assumed to be noncooperative, a poor fit to the data is observed (Figure 9, red curves). The simplest model that describes the data yields two very different dissociation constants for the first and second

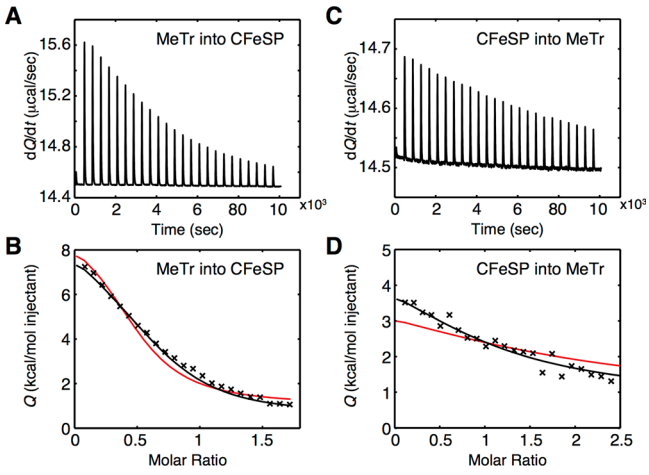

Figure 9. ITC analysis of subunit binding cooperativity under assay conditions. (A) Raw measured heat changes as a function of time injecting 800 μM MeTr into 83 μM CFeSP and (B) corresponding normalized measured heats of injection. (C) Raw measured heat changes as a function of time injecting 153 μM CFeSP into 10.95 μM MeTr and (D) corresponding normalized measured heats of injection. A global analysis of the data assuming noncooperative binding of CFeSP to MeTr yields a poor fit (red lines in B and D, χ^2 = 8.60). Allowing for cooperativity in the global model leads to a significantly improved fit (black lines in B and D, χ^2 = 1.65), yielding an enthalpy change of ΔH of 4.9 [4.1−6.1] kcal/mol for the 1:1 complex and K_ds of 7.7 [4.4−12.8] and 111 [90−143] μM for the first and second binding events, respectively. Uncertainties are asymmetric 95% confidence intervals.

dx.doi.org/10.1021/ja3055782 | J. Am. Chem. Soc. 2012, 134, 17945−17954

binding events of 7.7 and 111 μM, respectively (Figure 9, black curves). In this model, the difference in binding free energy is attributed to an increased entropic cost ($-T\Delta\Delta S$ of 1.56 kcal/mol) for the second binding event.

Complex Formation under Crystallization Conditions. Although a 1:1 CFeSP/MeTr complex is predominant under assay conditions, crystal structures of CFeSP and MeTr in complex depict a 2:1 stoichiometry. Thus, we investigated whether complex formation is affected by the presence of the crystallization precipitant in solution. The subunit titration experiment was repeated in a solution that mimics the crystallization conditions, a 2:1 volumetric mixture of the assay conditions and the crystallization precipitant: 100 mM bis-Tris pH 6.5, 100 mM calcium acetate, 9% polyethylene glycol monomethylether (PEG MME) 5000, and 20% glycerol.[9] CFeSP was titrated into 50 μM MeTr under crystallization conditions, yielding reasonably linear Guinier curves as before (Figure 2F). Linear combinations of the uncomplexed proteins, the 1:1 complex, and the 2:1 complex described above provide good fits to the scattering profiles (Figure 7B). The existence of four, rather than three, significant species is supported by SVD analysis (Figure S3B). Again, the apparent volume fractions of each species display physically reasonable trends with increasing CFeSP concentration (Figure 7D). As in the previous titration experiment under assay conditions, free MeTr is consumed to form CFeSP/MeTr complexes as CFeSP is added. However, under crystallization conditions, both 1:1 and 2:1 complexes are formed. At low CFeSP:MeTr ratios, the 1:1 complex is favored, while the larger 2:1 complex becomes favored in the presence of excess CFeSP (Figure 7D).

To further compare the two titration experiments (Figure 7A,B), scattering profiles were converted into pair-distance distributions, $P(r)$, by the indirect Fourier transform method implemented in GNOM[28] (Figure 10A). The maximum dimension, D_{max}, was determined by allowing $P(r)$ to naturally approach zero without constraints. Under assay conditions, D_{max} values do not exceed 100 Å (the maximum dimension of the 1:1 complex) even with excess CFeSP (Figure 10A, blue curves). However, under crystallization conditions, D_{max} increases smoothly to 140 Å, while the peak position remains largely unchanged (Figure 10A, red curve), consistent with the presence of an elongated species similar in length to the 2:1 complex. These results lend additional support to the deconvolution analyses, which indicate that the 1:1 complex is the dominant form in solution under assay conditions, while the 2:1 complex can additionally be formed under crystallization conditions.

In a separate experiment, we examined the contributions of each ingredient of the crystallization condition to the oligomerization state of the CFeSP/MeTr complex. Each ingredient was individually added to 2:1 molar mixtures of CFeSP and MeTr. Of all ingredients, a major effect on the oligomerization state was observed only with PEG MME 5000, a macromolecular crowding agent present at a final concentration of 3% w/v in the crystallization condition. Increasing the concentration of PEG MME 5000 up to 9% leads to a D_{max} approaching 140 Å, indicative of the formation of the 2:1 complex (Figure 10B). Further increasing the PEG MME 5000 concentration to 12% leads to an additional peak exceeding a D_{max} of 140 Å, suggestive of even higher-order oligomerization or nonspecific aggregation (Figure 10B, purple curve).

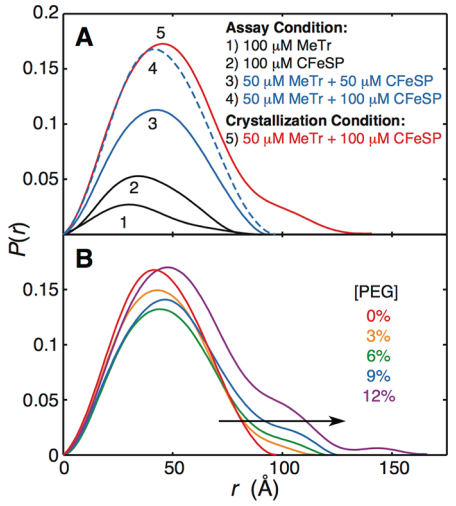

Figure 10. Pair-distance distribution, $P(r)$, plots of species in CFeSP/MeTr mixtures. (A) Under assay conditions, the maximum particle dimensions, D_{max}, for the free subunits are <100 Å and consistent with the crystal structures of the individual proteins.[9,11] D_{max} values for CFeSP/MeTr mixtures also do not exceed 100 Å under assay conditions (blue curves), while D_{max} extends to ~140 Å under crystallization conditions (red curve). This result is consistent with the 1:1 CFeSP/MeTr complex being the largest species under assay conditions, even in the presence of excess CFeSP (blue dashed curve), and the appearance of the 2:1 CFeSP/MeTr complex under crystallization conditions. (B) Titration of PEG MME 5000 into a solution with 100 μM CFeSP and 50 μM MeTr leads to an increase in D_{max} from ~100 Å toward ~140 Å. At the maximum PEG concentration tested, 12%, even higher order oligomerization is detected (D_{max} > 150 Å). For comparison, the PEG MME 5000 concentration is 3% in the crystallization condition.

DISCUSSION

Using anaerobic SAXS and ITC, we have probed the quaternary organizations of CFeSP and MeTr components of B_{12}-dependent methyl transfer, both alone and in complex. We find that although CFeSP and MeTr maintain their respective heterodimeric and homodimeric associations when alone in solution, two different CFeSP/MeTr structures are possible upon complex formation. Under assay conditions, the complex with 1:1 stoichiometry is strongly favored, leaving one MeTr active site unused. The observed ionic strength dependence suggests that specific CFeSP−MeTr interactions, composed of a salt bridge and hydrogen bonds, are intact in the 1:1 complex (Figure 10A,B). However, under the CFeSP/MeTr crystallization conditions, both 1:1 and 2:1 complexes form, the latter of which resembles the CFeSP/MeTr crystal structure and is preferred at excess CFeSP concentrations. Further analysis indicates that formation of the 2:1 complex is enabled by PEG, a macromolecular crowding agent in the crystallization solution. While crowding is well-known to promote homo-oligomeric association,[29] to the best of our knowledge, these results represent the first example of a hetero-oligomeric complex in which the subunit stoichiometry is affected by crowding.

Negative cooperativity was unexpectedly observed in the binding of CFeSP to MeTr under solution conditions that are used to assay enzyme activity,[9,18] while such behavior is lost in the presence of PEG. With CFeSP able to bind opposing sides of the MeTr homodimer, the molecular basis for negatively cooperative behavior is not immediately obvious. Closer consideration of the crystal structures of the 2:1 complex,

dx.doi.org/10.1021/ja3055782 | J. Am. Chem. Soc. 2012, 134, 17945−17954

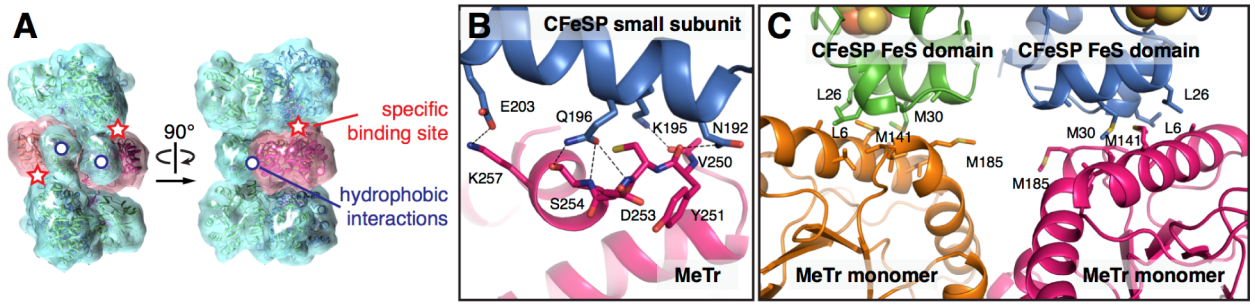

Figure 11. Interaction interfaces between CFeSP and MeTr observed in crystal structures of the complex.[9] (A) The small subunit and the Fe_4S_4 domain of each CFeSP (cyan) interact with MeTr (pink) at two distinct locations. CFeSP binds specifically to sites on opposing sides of the MeTr homodimer (red ☆) and makes nonspecific interactions with closely spaced hydrophobic regions on the TIM barrel walls (blue ○). (B) Close-up view of the specific CFeSP binding site on MeTr (☆ in (A)), consisting of hydrogen bonds and a salt bridge between Glu203 of the CFeSP small subunit and Lys257 of MeTr. (C) Nonspecific CFeSP−MeTr interactions are made by hydrophobic residues on the CFeSP Fe_4S_4 domains and the MeTr TIM barrel walls (○ in (A)).

however, shows that each CFeSP makes both specific and nonspecific interactions with MeTr (Figure 11A),[9] and while the sites of the specific interactions are far removed from each other on the different ends of the MeTr homodimer (Figure 11A,B), the locations of the nonspecific interactions are adjacent (Figure 11C). In particular, these nonspecific interactions are made between the Fe_4S_4 domain of CFeSP and the hydrophobic patches on the sides of MeTr, placing the otherwise mobile Fe_4S_4 domains of both CFeSPs side by side in close proximity (Figures 11A,C). Thus, in the absence of a macromolecular crowding agent, the placement of a second CFeSP Fe_4S_4 domain adjacent to the first may be unfavorable, leading to the observed negativity cooperativity. Such a mechanism is supported by our ITC analysis, which indicates that the negative cooperativity can be explained by an increased entropic cost for the binding of a second CFeSP to a 1:1 complex.

It is interesting to consider whether this negative cooperativity in the binding of CFeSP to MeTr will occur in the organism or whether in the crowded cellular environment of this mildly thermophilic acetogen both 1:1 and 2:1 complexes will form. Importantly, both 1:1 and 2:1 CFeSP/MeTr complexes are active. Here, our data show that the solution conditions used in activity assays[9,18] give rise to the 1:1 complex, meaning that published kinetic data for this methyl transfer reaction are reporting the activity of the 1:1 complex. Previously, we have used a spectroscopic assay to show that crystals that consist solely of the 2:1 complex are active.[9] Thus, although activities of solution and crystallized proteins cannot easily be kinetically compared, both complexes may have physiological relevance. While the 2:1 complex is more efficient in terms of utilizing both MeTr active sites, CFeSP must also partner with other enzymes in the Wood−Ljungdahl pathway. Negative cooperativity may have importance in pathway dynamics by allowing for more efficient dissociation of methylated CFeSP from MeTr and facilitate its binding to acetyl-CoA synthase (ACS) to perform the subsequent methyl transfer step.

CONCLUSION

The ability of CFeSP and MeTr to form protein−protein complexes with differing oligomeric states is intriguing in terms of the potential biotechnological applications of the Wood−Ljungdahl pathway. This pathway, used by acetogens for autotrophic growth on CO in addition to CO_2/H_2,[1,2] is receiving renewed attention for possible application in the clean production of desirable multicarbon compounds, such as biofuels, from industrial waste gases or synthesis gases produced from renewable biomass.[4,5,30,31] Our work suggests that the protein−protein interactions made by MeTr, CFeSP, and ACS are sensitive to protein expression levels and may be important variables in optimizing such engineering efforts. Finally, our work underscores the importance of distinguishing protein interactions in the crystal, in solution, and in the cell. Solution behavior revealed by SAXS provides a first step toward understanding the detailed but static information gained by crystallography in a physiological context.

EXPERIMENTAL PROCEDURES

Protein Expression and Purification. CFeSP was expressed and purified anaerobically from *M. thermoacetica* ATCC 39073 as described,[21] except for the following modifications: All anaerobic procedures were performed in a Vacuum Atmospheres chamber, under conditions of perpetual O_2 concentration below 2 ppm. CFeSP was purified from cell extracts from ∼160 g of wet cell weight of cells using an initial DEAE-cellulose resin and subsequent high-resolution Q-sepharose anion exchange chromatography followed by phenyl-sepharose hydrophobic interaction chromatography. Fractions containing CFeSP were analyzed by SDS-PAGE and concentrated and buffer exchanged using Amicon Ultra centrifugal concentrators in an anaerobic chamber (Coy Laboratories). The enzyme was characterized and assayed by UV−vis absorption spectroscopy by measuring the oxidation and methylation states of the cobamide, using an Applied Photophysics anaerobic UV−vis spectrophotometer. MeTr was expressed and purified aerobically from recombinant *Escherichia coli* as described[10] and made anaerobic by buffer exchange in the anaerobic chamber after purification. The concentrations of CFeSP and MeTr protein samples were determined using the Rose−Bengal method,[23] and the proteins were stored in assay buffer (50 mM Tris-HCl, pH 7.6, 100 mM NaCl, 2 mM dithiothreitol). All molar protein concentrations are dimeric concentrations (i.e., MeTr homodimer and CFeSP heterodimer). Samples were of the same as-isolated form as previously used in crystallization of CFeSP/MeTr complexes,[9] with the CFeSP B_{12} cobalt atom primarily in the Co(II) oxidation state.

SAXS. SAXS was performed at the Cornell High Energy Synchrotron Source (CHESS) G1 station using a 250 mm square X-ray beam with a flux of several 10^{12} photons/s/mm^2 at 9.6 or 10.5 keV. Data were collected at room temperature on a custom 1024 × 1024 pixel CCD detector similar to that described previously[32] with a sample-to-detector distance of ∼1 m. All samples were prepared in an anaerobic chamber (Coy Laboratories) under a N_2/H_2 atmosphere (94%/6%). For *ab initio* shape reconstructions of MeTr and CFeSP and for determination of relative protein concentrations, the protein solutions and matching buffers were contained in 2 mm path length

dx.doi.org/10.1021/ja3055782 | J. Am. Chem. Soc. 2012, 134, 17945−17954

acrylic cells (ALine Inc.) with 7.5 μm Kapton windows (Chemplex)[33] that were sealed with epoxy within the anaerobic chamber to maintain anaerobic conditions prior to data collection. To prevent potential oxygen permeation through the Kapton windows, which occurs over long time scales (>15 min), each acrylic cell was stored in an individual airtight container, which was not opened until immediately before data collection. The oxygen permeability of epoxy-sealed Kapton windows was tested separately by monitoring the oxidation of reduced methyl viologen solution with a microscpectrophotometer described previously.[9] The time course of the methyl viologen absorbance indicates that over 5−10 min (the maximum duration that the SAXS cells were exposed to air), the samples remain ∼95% as anaerobic as initial conditions. For all other experiments, epoxy-sealed glass and boron-rich glass X-ray capillaries (Charles Supper) of similar path lengths were used instead. While glass capillaries are not ideal sample cells for SAXS, they provide superior oxygen impermeability compared to the acrylic cells, as assessed by use of methyl viologen, and display sufficiently low parasitic scattering at low q relative to the protein scattering.

Several 1 and 2 s exposures were taken separated by 10 s pauses, where the entire sequence did not exceed 5 min per sample. Exposures that did not display apparent radiation-induced changes were averaged after previously described image correction procedures.[33] The corrected scattering images were integrated about the beam center and normalized by the transmitted intensities measured by a PIN diode beamstop.[33] Background scattering was subtracted from the protein solution scattering to produce the one-dimensional protein scattering profile, $I(q)$, as a function of q, where $q = 4\pi/\lambda \sin\theta$; 2θ is the scattering angle, and λ is the X-ray wavelength.

A Guinier approximation was applied to the low q region of the scattering profile:

$$I(q) \approx I(0)e^{-R_g^2 q^2/3}$$

where the radius of gyration, R_g, and the forward scattering intensity, $I(0)$, were determined from a linear fit to the Guinier plot, $\ln(I)$ vs q^2, for the q range that satisfies the $q \cdot R_g$ <1.3 condition.[34]

The pair distance distribution function, $P(r)$, was calculated from the experimental $I(q)$ with the indirect Fourier transform method[19] implemented in the program GNOM.[28] The maximum electron pair distance (i.e., maximum protein dimension), D_{max}, was chosen where $P(r)$ naturally approached zero without constraints.[19] Low q data points that exhibited interparticle interference and high q data points with low signal-to-noise were omitted from this procedure. Low-resolution models of protein structures were generated from the GNOM outputs with a high-resolution limit of $q \cdot R_g \sim 8$ using the *ab initio* reconstruction program, DAMMIF.[35] The program DAMAVER[36] was used to align *ab initio* models, reject outliers, and average to produce the most probable models. Averaged models were aligned to crystal structures in the program SUPCOMB20.[37]

Theoretical scattering curves and R_g values were calculated from atomic coordinates using CRYSOL.[25] To generate the coordinates of the 1:1 complex, one of the two CFeSPs was simply removed from the structure of the 2:1 complex. Missing side chains in coordinate files were automatically generated in CNS,[38] and crystallographic heteroatoms were removed. For experiments with MeTr and CFeSP alone, theoretical scattering curves were fit to experimental scattering curves in CRYSOL (over the q range 0.018−0.25 Å^{-1}),[25] whereas linear combinations of theoretical scattering curves were fitted to titration data using a non-negative least-squares fitting algorithm implemented in the program OLIGOMER:[26]

$$I_{fit}(q) = \sum_i^N v_i I_i(q)$$

where $I_i(q)$ and v_i are the theoretical scattering curve and the apparent volume fraction for the i^{th} species, and N is the number of species. High q regions of the data (q > 0.16 Å^{-1}), which are sensitive to the quality of background subtractions, were omitted in this analysis. The cutoff for the maximum q was determined by comparisons of data collected in flat window cells and capillaries.

SVD analysis was used to determine the minimum number of significant species.[14,24] Using MATLAB (The MathWorks), a matrix of data, **A**, with columns consisting of scattering intensities for 50 μM MeTr, 25−75 μM CFeSP, and 50 μM MeTr + 10−150 μM CFeSP was decomposed as follows:

$$\mathbf{A} = \mathbf{U}\Sigma\mathrm{V}$$

where the columns of the matrix **U** contain the singular vectors (referred to as SVD states) and the SVD coefficients are the product of the singular value matrix, Σ, with the conjugate transpose of V.

ITC. ITC experiments were performed at 20 °C using a VP-ITC Micro Calorimeter (Microcal LLC, Northampton, MA, USA) installed in a Vacuum Atmospheres anaerobic chamber. MeTr and CFeSP were buffer exchanged into a modified assay buffer (50 mM Tris-HCl, pH 7.6, 100 mM NaCl, 0.5 mM dithiothreitol) using dialysis tubing under anaerobic conditions. In one experiment, 800 μM MeTr was titrated into 83.4 μM CFeSP, and in the other, 153 μM CFeSP was titrated into 10.95 μM MeTr. Collected data were initially processed with Microcal Origin. Global analysis of the processed data was performed in Sedphat[27] using a two-symmetric-site model. The reported uncertainties are 95% confidence intervals.

■ ASSOCIATED CONTENT

Supporting Information

Individual shape reconstructions of free CFeSP (Figure S1); residuals of multispecies fits to titration data under assay conditions (Figure S2); singular value decomposition of titration data under both assay and crystallization conditions (Figure S3); additional multispecies fits to titration data under assay conditions (Figure S4). This information is available free of charge via the Internet at http://pubs.acs.org/.

■ AUTHOR INFORMATION

Corresponding Author

cdrennan@mit.edu

Notes

The authors declare no competing financial interest.

■ ACKNOWLEDGMENTS

For assistance with SAXS data collection, we thank Mackenzie Firer-Sherwood (BU), Jeremy Setser (MIT), Marco Jost (MIT), Rebekah Bjork (MIT), and CHESS scientists Drs. Arthur Woll and Richard Gillilan. We thank Prof. Sol Gruner (Cornell) for access to SAXS equipment and Prof. Brian Crane (Cornell) for access to an anaerobic chamber. CHESS is supported by the NSF and NIH/NIGMS via NSF award DMR-0936384, and the MacCHESS resource is supported by NIH/NCRR award RR-01646. This work was supported by the National Institutes of Health grants K99GM100008 (N.A.), F32GM090486 (N.A.), GM69857 (C.L.D.), and GM39451 (S.W.R.). C.L.D. is a Howard Hughes Medical Institute Investigator.

■ REFERENCES

(1) Ragsdale, S. W. *Ann. N.Y. Acad. Sci.* **2008**, *1125*, 129.
(2) Ragsdale, S. W.; Pierce, E. *Biochim. Biophys. Acta* **2008**, *1784*, 1873.
(3) Drake, H. L.; Gössner, A. S.; Daniel, S. L. *Ann. N.Y. Acad. Sci.* **2008**, *1125*, 100.
(4) Phillips, J. R.; Clausen, E. C.; Gaddy, J. L. *Appl. Biochem. Biotechnol.* **1994**, *45*, 145.
(5) Slivka, R. M.; Chinn, M. S.; Grunden, A. M. *Biofuels* **2011**, *2*, 405.

(6) Vega, J.; Prieto, S.; Elmore, B.; Clausen, E.; Gaddy, J. *Appl. Biochem. Biotechnol.* **1989**, *20*, 781.
(7) Zhao, S.; Roberts, D. L.; Ragsdale, S. W. *Biochemistry* **1995**, *34*, 15075.
(8) Seravalli, J.; Zhao, S.; Ragsdale, S. W. *Biochemistry* **1999**, *38*, 5728.
(9) Kung, Y.; Ando, N.; Doukov, T. I.; Blasiak, L. C.; Bender, G.; Seravalli, J.; Ragsdale, S. W.; Drennan, C. L. *Nature* **2012**, *484*, 265.
(10) Doukov, T.; Seravalli, J.; Stezowski, J. J.; Ragsdale, S. W. *Structure* **2000**, *8*, 817.
(11) Doukov, T. I.; Hemmi, H.; Drennan, C. L.; Ragsdale, S. W. *J. Biol. Chem.* **2007**, *282*, 6609.
(12) Goetzl, S.; Jeoung, J. H.; Hennig, S. E.; Dobbek, H. *J. Mol. Biol.* **2011**, *411*, 96.
(13) Svetlitchnaia, T.; Svetlitchnyi, V.; Meyer, O.; Dobbek, H. *Proc. Natl. Acad. Sci. U.S.A.* **2006**, *103*, 14331.
(14) Ando, N.; Brignole, E. J.; Zimanyi, C. M.; Funk, M. A.; Yokoyama, K.; Asturias, F. J.; Stubbe, J.; Drennan, C. L. *Proc. Natl. Acad. Sci. U.S.A.* **2011**, *108*, 21046.
(15) van den Heuvel, R. H. H.; Svergun, D. I.; Petoukhov, M. V.; Coda, A.; Curti, B.; Ravasio, S.; Vanoni, M. A.; Mattevi, A. *J. Mol. Biol.* **2003**, *330*, 113.
(16) Hura, G. L.; Menon, A. L.; Hammel, M.; Rambo, R. P.; Poole, F. L.; Tsutakawa, S. E.; Jenney, F. E.; Classen, S.; Frankel, K. A.; Hopkins, R. C.; Yang, S.-J.; Scott, J. W.; Dillard, B. D.; Adams, M. W. W.; Tainer, J. A. *Nat. Methods* **2009**, *6*, 606.
(17) Jacques, D. A.; Trewhella, J. *Protein Sci.* **2010**, *19*, 642.
(18) Seravalli, J.; Ragsdale, S. W. *J. Biol. Chem.* **2008**, *283*, 8384.
(19) Glatter, O.; Kratky, O. In *Small Angle X-ray Scattering*; Glatter, O., Ed.; Academic Press: London, 1982; Vol. *119*−*165*.
(20) Fischer, H.; de Oliveira Neto, M.; Napolitano, H. B.; Polikarpov, I.; Craievich, A. F. *J. Appl. Crystallogr.* **2010**, *143*, 101.
(21) Ragsdale, S. W.; Lindahl, P. A.; Münck, E. *J. Biol. Chem.* **1987**, *262*, 14289.
(22) Roberts, D. L.; James-Hagstrom, J. E.; Garvin, D. K.; Gorst, C. M.; Runquist, J. A.; Bauer, J. R.; Haase, F. C.; Ragsdale, S. W. *Proc. Natl. Acad. Sci. U.S.A.* **1988**, *86*, 32.
(23) Elliott, J. I.; Brewer, J. M. *Arch. Biochem. Biophys.* **1978**, *190*, 351.
(24) Putnam, C. D.; Hammel, M.; Hura, G. L.; Tainer, J. A. *Q. Rev. Biophys.* **2007**, *40*, 191.
(25) Svergun, D.; Barberato, C.; Koch, M. H. J. *J. Appl. Crystallogr.* **1995**, *28*, 768.
(26) Konarev, P. V.; Volkov, V. V.; Sokolova, A. V.; Koch, M. H. J.; Svergun, D. I. *J. Appl. Crystallogr.* **2003**, *36*, 1277.
(27) Houtman, J. C. D. J.; Brown, P. H. P.; Bowden, B. B.; Yamaguchi, H. H.; Appella, E. E.; Samelson, L. E. L.; Schuck, P. P. *Protein Sci.* **2007**, *16*, 30.
(28) Svergun, D. I. *J. Appl. Crystallogr.* **1992**, *25*, 495.
(29) Phillip, Y.; Sherman, E.; Haran, G.; Schreiber, G. *Biophys. J.* **2009**, *97*, 875.
(30) Abrini, J.; Naveau, H.; Nyns, E. J. *Arch. Microbiol.* **1994**, *161*, 345.
(31) Abubackar, H. N.; Veiga, M. C.; Kennes, C. *Biofuels, Bioprod. Biorefin.* **2011**, *5*, 93.
(32) Tate, M. W.; Eikenberry, E. F.; Barna, S. L.; Wall, M. E.; Lowrance, J. L.; Gruner, S. M. *J. Appl. Crystallogr.* **1995**, *28*, 196.
(33) Ando, N.; Chenevier, P.; Novak, M.; Tate, M. W.; Gruner, S. M. *J. Appl. Crystallogr.* **2008**, *41*, 167.
(34) Svergun, D. I.; Koch, M. H. J. *Rep. Prog. Phys.* **2003**, *66*, 1735.
(35) Franke, D.; Svergun, D. I. *J. Appl. Crystallogr.* **2009**, *42*, 342.
(36) Volkov, V. V.; Svergun, D. I. *J. Appl. Crystallogr.* **2003**, *36*, 860.
(37) Kozin, M. B.; Svergun, D. I. *J. Appl. Crystallogr.* **2001**, *34*, 33.
(38) Brünger, A. T.; Adams, P. D.; Clore, G. M.; DeLano, W. L.; Gros, P.; Grosse-Kunstleve, R. W.; Jiang, J. S.; Kuszewski, J.; Nilges, M.; Pannu, N. S.; Read, R. J.; Rice, L. M.; Simonson, T.; Warren, G. L. *Acta Crystallogr., Sect. D: Biol. Crystallogr.* **1998**, *54*, 905.